



Velocity Dispersion of the Open Cluster NGC 2571 by Radial Velocities and Proper Motions

Maxim V. Kulesh¹ , Aleksandra E. Samirkhanova¹, Giovanni Carraro² , Joao V. Sales-Silva³ , Roberto Capuzzo Dolcetta⁴, and Anton F. Seleznev¹

¹ Ural Federal University, 51 Lenin Street, Ekaterinburg, 620000, Russia

² Dipartimento di Fisica e Astronomia, Università di Padova, Vicolo Osservatorio 3, I-35122, Padova, Italy; giovanni.carraro@aas.org

³ Observatório Nacional/MCTIC, R. Gen. José Cristino, 77, 20921-400, Rio de Janeiro, Brazil

⁴ Dipartimento di Fisica, Sapienza Università di Roma, P.le A. Moro 5, I-00165 Roma, Italy

Received 2024 January 24; revised 2024 February 25; accepted 2024 March 10; published 2024 April 12

Abstract

We use a kernel density estimator method to evaluate the stellar velocity dispersion in the open cluster NGC 2571. We derive the 3D velocity dispersion using both proper motions as extracted from Gaia Data Release 3 and single-epoch radial velocities as obtained with the instrument FLAMES at ESO's Very Large Telescope. The mean-square velocity along the line of sight is found to be larger than the one in the tangential direction by a factor of 6–8. We argue that the most likely explanation for such an occurrence is the presence of a significant quantity of unresolved binary and multiple stars in the radial velocity sample. Special attention should be paid to single-line spectroscopic binaries (SB1) since in this case we observe the spectral lines of the primary component only, and therefore the derived radial velocity is not the velocity of the binary system center of mass. To investigate this scenario, we performed numerical experiments varying the fractional abundance of SB1 in the observed sample. These experiments show that the increase of the mean-square radial velocity depends on the fractional abundance of SB1 to a power in the range [0.39, 0.45]. We used the 3D velocity dispersion obtained by the dispersions in the tangential directions and the assumption that the radial velocity dispersion is the same as a tangential one to estimate the virial cluster mass and the cluster mass, taking into account the gravitational field of the Galaxy and the nonstationarity of the cluster. These estimates are $650 \pm 30 M_{\odot}$ and $310 \pm 80 M_{\odot}$, respectively, in substantial agreement with the photometric cluster mass.

Unified Astronomy Thesaurus concepts: Open star clusters (1160); Binary stars (154)

1. Introduction

The precise determination of the mass of star clusters is an important asset for many astrophysical applications. For instance, the cluster stellar mass is necessary to study the cluster dynamics, to evaluate whether the cluster is bound or not. Moreover, in the case of extremely young clusters, their actual mass is key to evaluate the star formation efficiency.

It is customary to estimate the star cluster mass by two standard methods.

First, the cluster mass can be determined either through the cluster member list or by utilizing the cluster luminosity function and adopting a mass–luminosity relation (Seleznev et al. 2017). The term “photometric mass” corresponds to the mass obtained this way. To this end, one needs to resort to theoretical isochrones. One serious problem in this procedure is the difficulty to evaluate reliably the uncertainty of the resulting mass. To overcome this obstacle, one can use the isochrone tables of different authors or derive the error from the analytical expression for the mass–luminosity relation as given, for example, by Eker et al. (2015).

We note that the photometric mass represents only a lower limit of the real cluster mass, because the lower end of the luminosity function, the number of invisible remnants of massive stars, and the fraction of unresolved binary and

multiple stars are usually unknown (Seleznev 2016a; Borodina et al. 2019, 2021).

The second method to evaluate the cluster mass relies on knowledge of the velocity dispersion of stars in the cluster (more precisely, the mean-squared of their velocity with respect to the cluster center-of-mass velocity). One can use a simple formula for the “virial” mass or the formula of Danilov & Loktin (2015) that takes into account the nonstationarity of the cluster and the influence of the Galactic gravitational field. The terms “virial mass” or “dynamical mass” are typically used in this case. In principle, this latter approach takes into account all cluster stars, and therefore would present an advantage with respect to the photometric estimate. However, this method also presents some difficulties. First, one should determine some structural characteristics of the cluster, like the cluster radius, which appear in the virial equation. To do this accurately, we need to obtain the cluster spatial density and use some numerical modeling (Seleznev et al. 2017). Second, for a good evaluation of the intrinsic velocity dispersion, one has to take into account the errors of the radial velocities and of the proper motions of stars. The third problem is the contamination of the sample of radial velocities by single-line spectroscopic binaries (SB1) since, in many cases, only one epoch of radial velocity observations is available. In this case, we see only the spectral lines of the bright (primary) component of the binary and, consequently, we cannot recognize this star as a binary with a single observation only. Then, the shift of the spectral lines in the spectrum will originate both from the binary system barycenter motion and from the motion of the primary component around the barycenter. Of course, these binaries cannot be distinguished from single stars



Original content from this work may be used under the terms of the [Creative Commons Attribution 4.0 licence](https://creativecommons.org/licenses/by/4.0/). Any further distribution of this work must maintain attribution to the author(s) and the title of the work, journal citation and DOI.

with just single-epoch observations. Consequently, in the case of a single-epoch observation, the observed radial velocity will deviate from the radial velocity of the binary system barycenter. As a result, we would derive a radial velocity dispersion larger than the real one. Seleznev et al. (2017) propose that this could be a plausible interpretation of the discrepancy between the estimates of photometric and dynamical masses in the open cluster NGC 4337.

The inflation of the velocity dispersion induced by unresolved binaries in star clusters has been confirmed also by numerical N -body experiment; see, e.g., Rastello et al. (2020).

In this study, we propose a way to amend this bias relying on the kernel density estimator (KDE; Silverman 1986; Seleznev 2016b) statistical method and apply it to the open cluster NGC 2571. We take the data for the proper motions of stars in this cluster from the Gaia Data Release 3 (DR3) catalog (Gaia Collaboration et al. 2023) and use the original data on the radial velocities of its stars as obtained with the Very Large Telescope (VLT). We assume for NGC 2571's distance to the Sun 1293 ± 46 pc following the catalog of Dias et al. (2021).

The rest of this paper is structured as follows. In Section 2, we describe the observational data; Section 3 gives a description of our method to evaluate the intrinsic velocity dispersion of stars in a cluster and its application to NGC 2571; in Section 4, we perform numerical modeling of the sample of radial velocities with different contents of SB1 and investigate the dependence of the velocity dispersion on the fraction of SB1 systems in the sample. Section 5 is dedicated to the mass estimates of NGC 2571. Finally, Section 6 is devoted to discussion of the results.

2. Observational Data

2.1. Astrometry

In this study, we extract proper-motion components from the Gaia DR3 catalog (Gaia Collaboration et al. 2016, 2023). In order to determine the tangential velocity dispersions, we use the samples of the probable cluster members derived by Cantat-Gaudin et al. (2020) and Hunt & Reffert (2023). Since the catalog of Cantat-Gaudin et al. (2020) contains proper motions from Gaia Data Release 2 (Gaia Collaboration et al. 2018), we replaced them with Gaia DR3 proper motions by cross-correlating the Cantat-Gaudin et al. (2020) list and the Gaia DR3 catalog (Gaia Collaboration et al. 2023). For both sources, we considered as bona fide cluster members those stars having a membership probability larger than 0.5.

2.2. Radial Velocities

Radial velocities for NGC 2571 stars were obtained using the FLAMES spectrograph on board UT2 at the ESO's Paranal Observatory on the night of 2016 January 22. Observations were carried out under $1.''3$ seeing and thin atmospheric conditions. One 45 minute long exposure was taken and the data were then pre-reduced using the observatory pipeline.

We used the GIRAFFE advanced data products processed by ESO Phase 3, which prepares and validates ESO science data. The spectra were reduced via the standard ESO GIRAFFE pipeline (giscience v2.14.2; Blecha et al. 2000), which consists of bias and dark correction, localization of the fibers on the detector, flat-fielding, spectrum extraction, and wavelength calibration. After giscience reduction, the ESO Phase 3 performed heliocentric correction in the wavelength. We also

manually inspected and cleaned the cosmic rays in each spectrum using IRAF's `splot` task. Finally, we normalized the stellar spectra through IRAF's `continuum` task.

We computed radial velocities and associated uncertainties of the cluster stars by cross-correlating the normalized spectra with a synthetic spectrum of similar stellar parameters from Munari et al. (2005). For this, we used IRAF's `FXCOR` task, which implements the Fourier cross-correlation method developed by Tonry & Davis (1979). The `FXCOR` task estimated the radial velocities by fitting the largest peak of the cross-correlation function, with the radial velocity determined by the peak center position. The radial velocity uncertainties were estimated using the fitted peak height and the antisymmetric noise, as described in Tonry & Davis (1979). Finally, we obtained a list of 78 stars with radial velocities in the field of NGC 2571. Then, we selected stars that could be members of the cluster. To do this, we used the mean value of the cluster proper motion from the Dias et al. (2021) catalog and selected stars with $\mu_\alpha \in [-5.9, -3.9] \text{ mas yr}^{-1}$ and $\mu_\delta \in [3.3; 5.3] \text{ mas yr}^{-1}$. These ranges for the proper motions correspond to $\pm 6.2 \text{ km s}^{-1}$, with the assumed cluster distance of 1293 pc. This is much larger than the typical internal mean-square velocity in open clusters. We ended up with 34 stars having radial velocities with the proper motions in this range. We consider these 34 stars as candidate cluster members and use them to evaluate the cluster radial velocity dispersion.

3. Evaluation of the Intrinsic Velocity Dispersion for NGC 2571

The various formulas to derive the cluster dynamical mass (see above and below) are all based on the mean-square velocity of the cluster stars. Usually, one computes the mean-square velocity in the cluster through the formula

$$\langle v^2 \rangle = \frac{1}{n} \sum_{i=1}^n (v_i - \langle v \rangle)^2, \quad (1)$$

where $\langle v \rangle$ is the velocity of the cluster center of mass, which we assume to be the mean velocity of the cluster stars. Note that in the above formula v can be either the 3D absolute value of the spatial velocity of the star or its radial velocity, or a component of the tangential velocity. The square root of $\langle v^2 \rangle$ is referred to as a velocity dispersion.

In the mathematical statistics Equation (1) corresponds to the biased estimate of the dispersion σ^2 , which is a parameter of the Gaussian (normal) distribution. The unbiased estimate of the dispersion σ^2 differs by a normalization factor, $(n-1)$, in the denominator instead of n . In this work, we neglect this difference and consider $\langle v^2 \rangle = \sigma^2$. Consequently, we will refer to a square root of the unbiased dispersion σ^2 also as the velocity dispersion.

The squared velocity dispersion is $\sigma^2 = \sigma_r^2 + \sigma_\alpha^2 + \sigma_\delta^2$, where σ_r , σ_α , and σ_δ are, respectively, the dispersion of the radial velocities, the dispersion of the velocities in the direction of the R.A., and the dispersion of the velocities in the direction of the decl. Clearly, in the assumption of spherical symmetry in velocity space, the total squared velocity dispersion is $\sigma^2 = 3\sigma_r^2$.

Of course, with the aim of determining the velocity dispersion from Equation (1), the problem of the correct accounting of the observational errors must be faced. We propose the following method to give a reliable evaluation of

the intrinsic velocity by a proper treatment of the observable distribution of velocities.

First, we note that observational errors widen the distribution of velocities. The situation is analogous to the widening of spectral lines by an instrumental profile or by the joint action of the various mechanisms of spectral-line broadening. In the last case, the resulting profile results from the convolution of functions corresponding to different broadening mechanisms (Gray 1976). We exploit this analogy and the properties of convolution.

If the functions describing the broadening mechanisms are all Gaussian, the result of the convolution will be a Gaussian function as well (Gray 1976). It is straightforward to show that in this case the dispersion of the resulting Gaussian function is the sum of the dispersions of all Gaussian functions corresponding to the broadening mechanisms.

Second, we plot the observable velocity distribution fitted using a KDE with a Gaussian kernel. The KDE is a straightforward method to obtain an estimate of the distribution function, giving a continuous and differentiable estimate. The advantages of this method as compared to the standard histogram techniques are listed in Silverman (1986), Merritt & Tremblay (1994), and Seleznev (2016b). In any case, this operation additionally broadens the observable velocity distribution. As a result, two mechanisms concur with the broadening of the intrinsic velocity distribution: the errors and the KDE. Then, we assume that the distribution of the velocity errors and the intrinsic distribution of velocities are both Gaussian. In this case, we can use the properties of convolution (see above):

$$\sigma_{\text{res}}^2 = \sigma_{\text{intrinsic}}^2 + \sigma_{\text{errors}}^2 + \sigma_{\text{KDE}}^2, \quad (2)$$

where σ_{res}^2 is the dispersion of the resulting Gaussian function of the observed velocity distribution, $\sigma_{\text{intrinsic}}^2$ is the dispersion of the intrinsic Gaussian velocity distribution, σ_{errors}^2 is the dispersion of the Gaussian distribution of the velocity errors, and σ_{KDE}^2 is the dispersion of the Gaussian kernel. Clearly, the ultimate goal is to obtain $\sigma_{\text{intrinsic}}$ from the other three terms in Equation (2). Having specified the parameters of the kernel, then σ_{KDE}^2 can be known. The σ_{res}^2 is evaluated through an approximation of the resulting distribution by a Gaussian.

We cannot plot the distribution of the observational errors because we know only the absolute magnitudes of the errors. Instead, we can investigate the distribution of the squared errors. Note that the quadratic function is a steadily increasing one. There is a theorem in mathematical statistics which allows one to get the analytical expression for the distribution of a steadily increasing function of a random variable (Taboga 2017). According to it, let the random variable ξ be distributed according to the density $f_{\xi}(x)$, and consider a steadily increasing function $g(x)$. Then, the random variable $\eta = g(x)$ has the density distribution $f_{\eta}(x) = (g^{-1}(x))' \cdot f_{\xi}(g^{-1}(x))$, where $g^{-1}(x)$ is an inverse function of g and $(g^{-1}(x))'$ is its derivative. The steadily increasing function g in this context is the square of the proper-motion error.

We consider the observational error as a random variable having a Gaussian distribution with mode m and dispersion σ_{errors}^2 . For the squared errors, we obtain (Taboga 2017)

$$f_{\eta}(x) = \frac{1}{2\sigma_{\text{errors}}\sqrt{2\pi x}} \cdot \exp\left(-\frac{(\sqrt{x} - m)^2}{2\sigma_{\text{errors}}^2}\right). \quad (3)$$

We approximate the distribution of the squared errors by Equation (3) and then determine the σ_{errors}^2 .

We applied this procedure to the distributions of tangential velocities and to the distribution of radial velocities of the probable members of the open cluster NGC 2571. The tangential velocities are connected with the corresponding proper motions by a relation $V_t = 4.74 \times \mu \times r$, where V_t is in kilometers per second, μ is the proper motion in milliarcseconds per year, and r is the heliocentric distance in kiloparsecs.

The distributions of the velocities and their squared errors plotted by the KDE are shown in Figure 1 by black lines. The best fits are shown by red lines: Gaussians for the velocity distributions and the functions in Equation (3) for the distributions of the velocity errors. The parameters of these approximations are summarized in Table 1.

One can readily see that the radial velocity dispersion is approximately 6–8 times larger than the velocity dispersion in both tangential directions. We explain this by pollution of the radial velocity sample by binary stars which are spectral binaries of the SB1 type. The next section describes the numerical experiment set up to confirm this point of view.

4. The Dependence of the Radial Velocity Dispersion on the Pollution of the Radial Velocities Sample by SB1 Stars

4.1. Problem Statement

In this section, we explore and evaluate the influence of SB1 stars on the radial velocity dispersion estimate. Let us consider a binary star system with the “primary” component mass M and the “secondary” component mass m defined by the mass ratio $q = m/M$. If the spectral lines of the secondary component in the spectrum of the binary are not visible, the binary can be interpreted as a single star. An attempt to take into account this potential bias is now described. Let us consider the relative orbit of the primary component around the secondary; see Figure 2 for an illustration. To make the analysis simpler, we consider the center of mass of the two stars as stationary. The position of the primary component in its relative orbit is uniquely determined by its true anomaly θ . The parameters of the orbit and the primary-component position are a , the semimajor axis of the relative orbit; e , the relative orbit eccentricity; ω , the position of the periastron with respect to the line of sight; and i , the inclination angle of the line of sight with respect to the orbital plane. We then use the simple Salpeter law for the distribution of the primary-component mass M to model SB1 systems:

$$F(M) \sim M^{-2.35}, \quad M \in [0.1, 10] M_{\odot}.$$

We take the distribution of q from our recent study (Malofeeva et al. 2022):

$$F(q) \sim q^{-0.53}, \quad q \in [0.1, 0.9].$$

As for the distribution of the semimajor axes a , we consider it uniform in the range of $[10, 3 \times 10^5]$ au (Tutukov & Kovaleva 2019).

The so-called *thermal* distribution is assumed for the distribution of eccentricities e (Jeans 1919): $F(e) \sim e$. The distributions of all angles are uniform: i in the range of $[0, \pi]$, ω and θ in the range of $[0, 2\pi]$.

At this point, the fundamental question to answer is: What is the distribution of the primary-component line-of-sight velocity relative to the center of mass of the binary system?

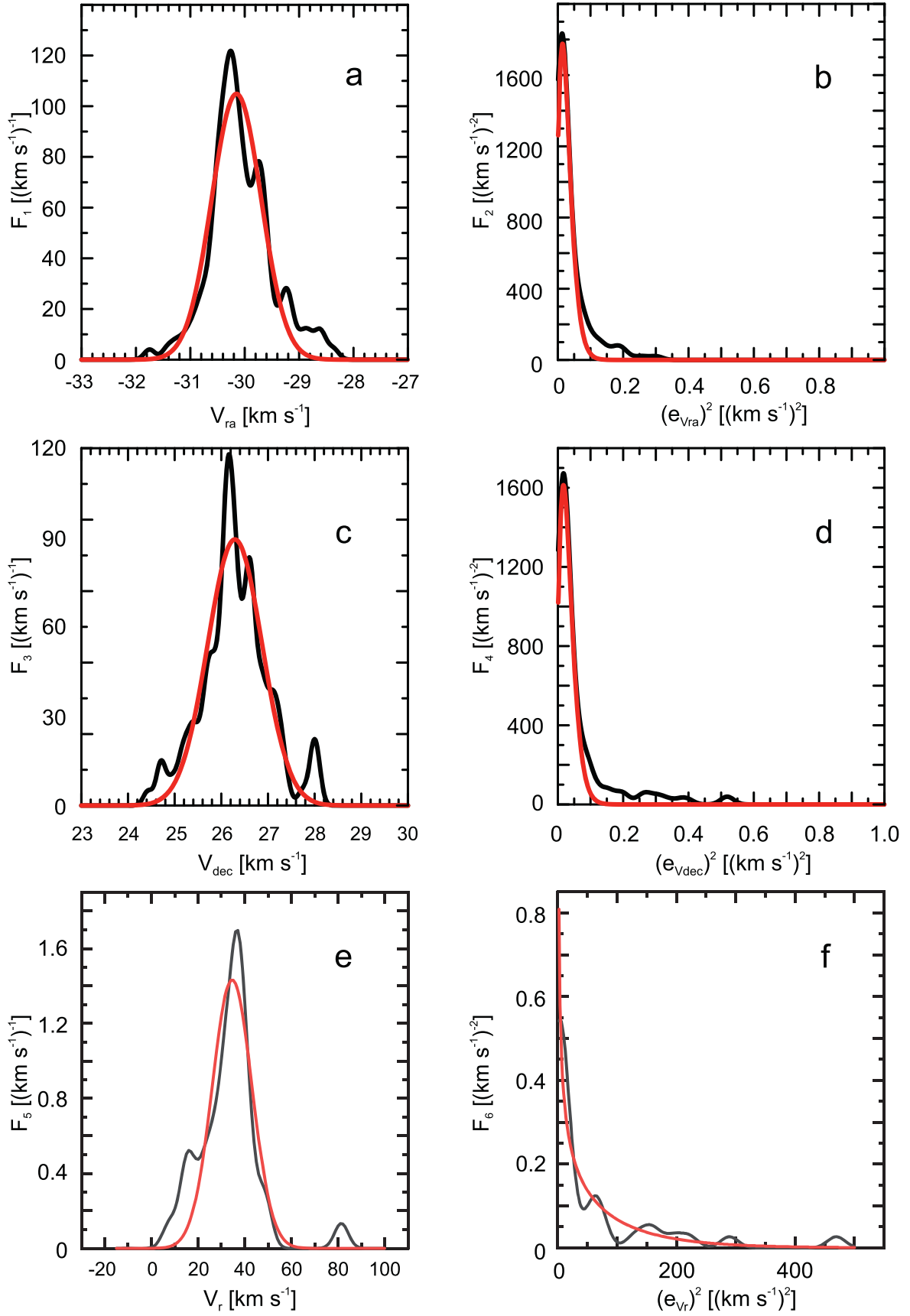


Figure 1. The left three-panel column reports the distributions of the tangential and radial velocities (black lines) together with their fit by Gaussian functions (red lines). The right three-panel column reports the distributions of the squared errors of velocities (black lines) and their fit by Equation (3) (red lines). Specifically, (a) distribution of the tangential velocities in the direction of the R.A., (b) distribution of their squared errors, (c) distribution of the tangential velocities in the direction of the decl., (d) distribution of their squared errors, (e) distribution of the radial velocities, and (f) distribution of their squared errors.

Table 1

The Results of Approximation (the Standard Deviations of a Resulting Distribution and Distribution of Errors), the Standard Deviation of the Gaussian Kernel, and the Intrinsic Standard Deviation of Velocity

Sample		σ_{res}	σ_{KDE}	σ_{errors}	$\sigma_{\text{intrinsic}}$
Radial velocities	V_r	8.5 ± 0.3	3	7.1 ± 0.2	3.5 ± 0.8
Cantat-Gaudin et al.	V_{ra}	0.454 ± 0.005	0.1	0.0647 ± 0.0003	0.438 ± 0.005
	V_{dec}	0.583 ± 0.010	0.1	0.0664 ± 0.0003	0.570 ± 0.010
Hunt & Reffert	V_{ra}	0.457 ± 0.003	0.1	0.0868 ± 0.0008	0.437 ± 0.003
	V_{dec}	0.558 ± 0.005	0.1	0.0859 ± 0.0006	0.542 ± 0.005

Note. All values given in kilometers per second.

4.2. Solution

To provide an answer to this question, we consider the case when the line of sight is not perpendicular to the orbital plane. Figure 2 sketches the orbit of the primary component M relative to the secondary component m and the projection of the line of sight onto the orbital plane.

The primary component M moves along the orbit with the semimajor axis a and eccentricity e in accordance with the solution of the unperturbed two-body problem with the full velocity \mathbf{v}_M . We should find the component of this velocity along the line of sight. Let α be the angle between the vector \mathbf{v}_M and the projection of the line of sight onto the orbital plane. Let Π be the orbit periastron, hence θ is the true anomaly of M .

Let IA be the intersection point of the line-of-sight projection and the line of apsides, then ω is the angle between the line-of-sight projection and the line of apsides. It is clear from Figure 2 that the angle between the radius vector of the primary component and the projection of the line of sight onto the orbital plane is

$$\gamma = \theta - \omega. \quad (4)$$

The orientation of the primary-component velocity vector \mathbf{v}_M relative to the line-of-sight projection can be calculated with its radial (v_r) and tangential (v_n) components relative to the primary-component radius vector. Let β be the angle between the primary-component radius vector and the primary-component velocity.

The v_r and v_n values depend on the true anomaly θ and eccentricity e :

$$v_r(\theta) = \frac{v_c}{\sqrt{1-e^2}} e \sin \theta, \quad (5)$$

$$v_n(\theta) = \frac{v_c}{\sqrt{1-e^2}} (1 + e \cos \theta), \quad (6)$$

where the circular velocity v_c depends on M , q , a , and on the gravitational constant $G = 887.125 \text{ au} \times (\text{km/s})^2 \times M_\odot^{-1}$ in appropriate units:

$$v_c = \sqrt{\frac{GM(1+q)}{a}}. \quad (7)$$

We obtain $\tan \beta$ by dividing Equation (6) by Equation (5), so we can evaluate β as

$$\beta = \arctan \frac{1 + e \cos \theta}{e \sin \theta} = \arctan \frac{\frac{1}{e} + \cos \theta}{\sin \theta}. \quad (8)$$

From Figure 2, one can readily see that $\alpha + \beta + \gamma = \pi$. Thus, substituting Equation (4), we obtain

$$\alpha = \pi - \beta - \gamma = \pi - \beta - \theta + \omega. \quad (9)$$

The value of v_M for any parameters can be inferred from the vis-viva equation for any v_c , a , and the radius vector modulus r :

$$v_M^2(r) = v_c^2 \left(\frac{2a}{r} - 1 \right), \quad (10)$$

where r is linked to θ , a , and e through the orbit equation (equation of an ellipse) in polar coordinates:

$$r(\theta) = \frac{a(1-e^2)}{1+e \cos \theta}. \quad (11)$$

We can evaluate $v_M(\theta)$ by plugging Equation (11) into Equation (10):

$$v_M(\theta) = v_c \sqrt{\frac{2(1+e \cos \theta)}{1-e^2} - 1} = v_c \sqrt{\frac{e^2 + 2e \cos \theta + 1}{1-e^2}}, \quad (12)$$

since we know both $v_M(\theta)$ and α . In this way, we can find the projection of the primary-component velocity onto the projection of the line of sight on the orbital plane:

$$v_1 = v_M(\theta) \cos \alpha. \quad (13)$$

Finally, the desired projection of the velocity of the primary component onto the line of sight is (see Figure 3)

$$v_2 = v_1 \cos i = v_M \cos \alpha \cos i. \quad (14)$$

Now, we must move to a reference frame associated with the center of mass of the binary system. For convenience, we perform this reference frame change in reverse order. Let us consider the coordinate system where the center of mass CM is stationary (see Figure 4(a)), then the primary component M has velocity \mathbf{v}_M , while the secondary component m has velocity \mathbf{v}_m . The total momentum of the system is equal to zero, so we can evaluate one velocity from another:

$$M\mathbf{v}_M + m\mathbf{v}_m = \mathbf{0}, \quad \mathbf{v}_m = -\frac{1}{q}\mathbf{v}_M. \quad (15)$$

To move to a reference frame with a stationary secondary component (see Figure 4(b)), we should subtract \mathbf{v}_m from the velocity of all points of the system. Then, the new velocity of the primary component \mathbf{v}'_M is

$$\mathbf{v}'_M = \mathbf{v}_M - \mathbf{v}_m = \left(\frac{q+1}{q} \right) \mathbf{v}_M. \quad (16)$$

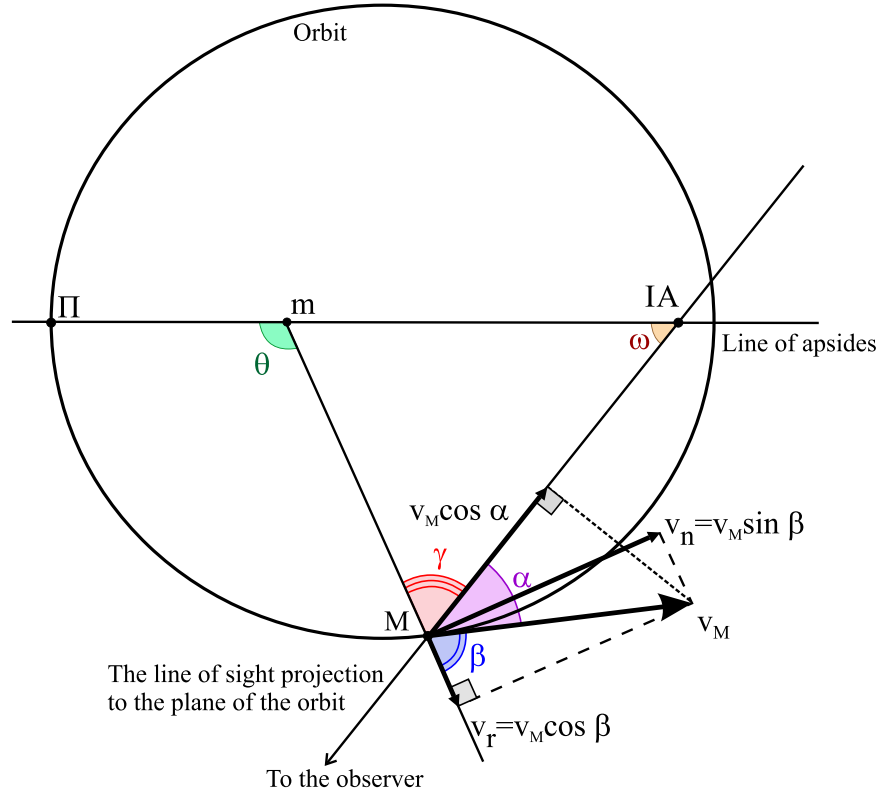


Figure 2. Orbit of the primary component M relative to the secondary component m . Π is the periastron. IA is the intersection point of the line-of-sight projection and the line of apsides. θ is the true anomaly.

Therefore, in order to get the velocity in the reference frame with stationary CM from the velocity on the orbit relative to the secondary component, we should multiply this velocity by a factor of $q/(1+q)$. As a result, we obtain the velocity of the primary component relative to the center of mass CM. In other words, this velocity will be an addition to the velocity of the binary system center of mass in case of a single observation of a SB1 system:

$$v_{SB1} = v_2 \frac{q}{1+q}. \quad (17)$$

In summary, we evaluate the radial velocity of one SB1 system following this procedure:

1. Initialize parameters q , M , a , e , ω , i , and θ from their corresponding distributions (see above).
2. Calculate the supplementary angle $\beta = \arctan [(1/e + \cos \theta)/\sin \theta]$ (see Equation (8)).
3. Calculate the supplementary angle $\alpha = \pi - \beta - \theta + \omega$ (see Equation (9)).
4. Calculate the circular velocity $v_c = \sqrt{GM(1+q)/a}$ (see Equation (7)).
5. Calculate the total velocity $v_M = v_c \sqrt{(e^2 + 2e \cos \theta + 1)/(1 - e^2)}$ (see Equation (12)).
6. Calculate the line-of-sight velocity $v_{SB1} = v_M q \cos \alpha \cos i / (1 + q)$ (see Equations (13), (14), and (17)).

4.3. The Influence of SB1 Systems on the Cluster Velocity Dispersion

First, we estimate the distribution of the primary-component radial velocities in SB1 systems relative to the center of mass of

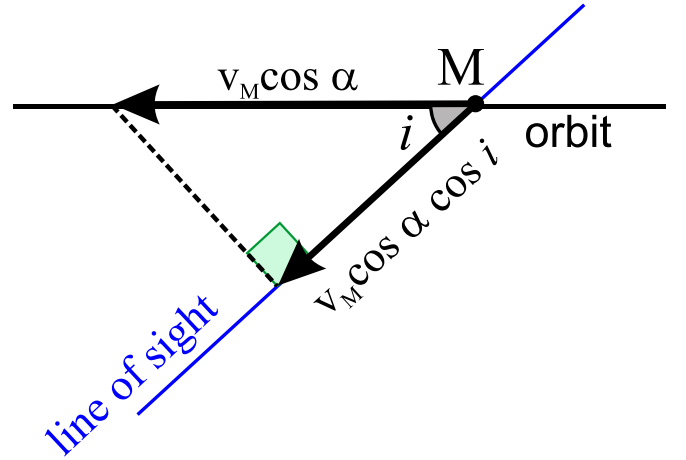


Figure 3. The plane passing through the primary component, containing the line of sight and perpendicular to the orbital plane. The angle i is an inclination of the line of sight to the orbital plane. $v_M \cos \alpha \cos i$ is the desired projection of the velocity of the primary component onto the line of sight.

the binary system. We achieve this by randomly generating a large number (100,000) of input parameters of such systems that satisfy the input distribution laws. The result is shown in Figure 5. The distribution is very narrow with wide tails. V_{SB1} is the difference between the line-of-sight projection of the primary component of the binary system and the radial velocity of the binary system mass center. In other words, it turns into an introduced error if we use the radial velocity of the SB1 considering it as a single star (note that we cannot distinguish SB1 systems with a single-epoch observation). This error results in overestimation of the radial velocity dispersion of the cluster.

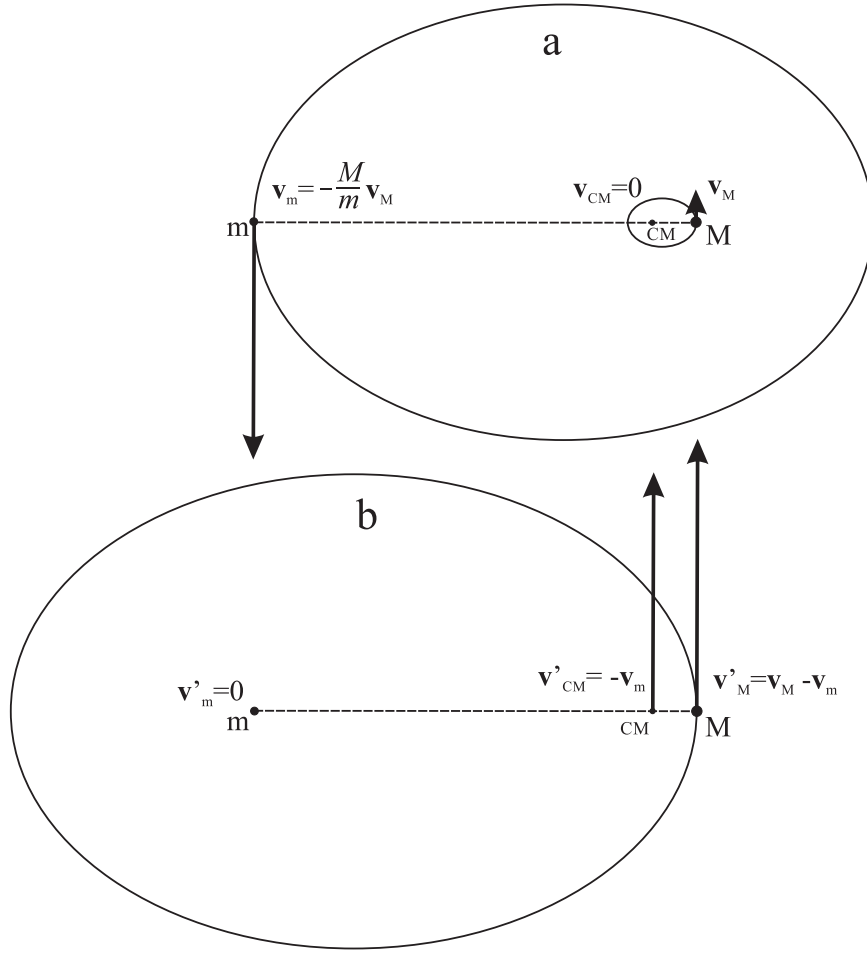


Figure 4. (a) Velocities of primary component M and secondary component m in a coordinate system associated with the center of mass CM , $\mathbf{v}_m = -(M/m)\mathbf{v}_M$, by conservation of momentum. (b) Velocities of primary component M and center of mass CM in a coordinate system associated with the secondary component.

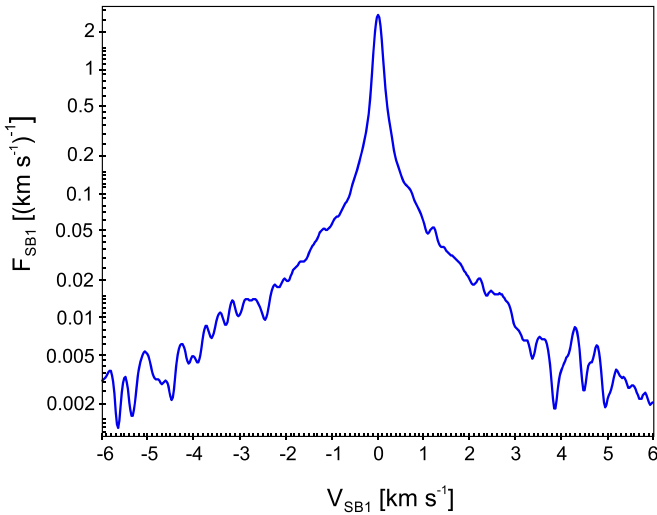


Figure 5. Distribution of the primary-component radial velocities in SB1 systems relative to the center of mass of the binary system in logarithmic scale.

Second, we answer the question: How does an additional SB1 radial velocity modify the cluster's radial velocity standard deviation (σ)? To answer this, we consider a simple cluster

model of $N=5000$ stars with a radial velocity standard deviation $\sigma_0 = 3^{-1/2} \approx 0.58 \text{ km s}^{-1}$. Every star is represented by its radial velocity v_r , generated from a normal distribution with a mean $\mu = 0 \text{ km s}^{-1}$ and $\sigma = \sigma_0$. Then, we specify the fraction of SB1 stars, f , among the cluster members. For every SB1 star, we add the additional velocity, v_{SB1} , generated from the distribution F_{SB1} , as shown in Figure 5. Taking these new velocities into account, we determine a new value of the mean-square velocity of the cluster model.

By generating around 1000 of such cluster models for every value of f , we get a violin plot for the dependence of the relative mean-square velocity σ/σ_0 on the SB1 fraction f . Figure 6 shows this plot in a square-root scale for seven values of the relative mean-square velocity. The horizontal lines at the vertical bars show 0%, 5%, 50%, 95%, and 100% quantiles of the distribution. We fitted quantiles 5%, 50%, and 95% with the following function:

$$\log \frac{\sigma}{\sigma_0} = a \log f + b,$$

where $\sigma_0 = 0.58 \text{ km s}^{-1}$ (see above), and σ is the rms velocity obtained after the addition of the fractional abundance f of SB1 binaries. σ_l and σ_u correspond to quantiles 5%, and 95%,

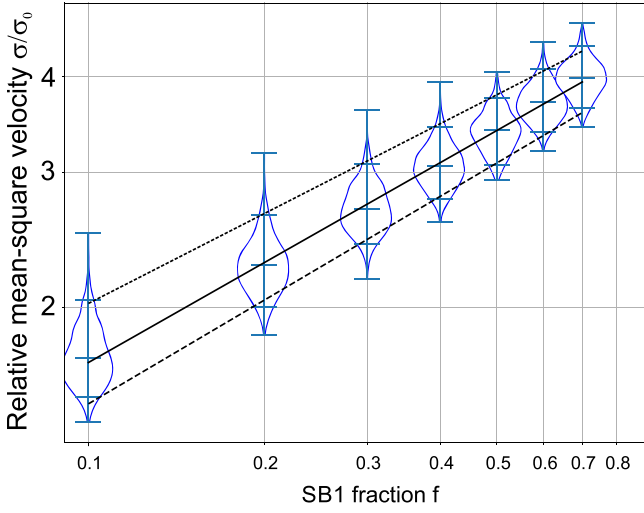


Figure 6. Violin plot for the dependence of the relative mean-square velocity σ/σ_0 on the SB1 fraction f in a square-root scale. The solid line is an approximation of the 50% quantile, the small-dashed line is an approximation of the 5% quantile, and the dashed line is an approximation of the 95% quantile.

respectively. The results are as follows:

$$\log \frac{\sigma}{\sigma_0} = 0.43 \log f + 0.66,$$

$$\log \frac{\sigma_l}{\sigma_0} = 0.45 \log f + 0.62,$$

$$\log \frac{\sigma_u}{\sigma_0} = 0.39 \log f + 0.70.$$

As expected, the relative mean-square velocity σ/σ_0 grows with f . If the velocity distribution of the primary components of SB1 binaries were Gaussian, one would expect

$$\sigma^2 = \sigma_0^2 + f\sigma_{\text{SB1}}^2,$$

in agreement with the properties of the convolution of two Gaussian distributions. In that case, the dependence of the relative mean-square velocity on the fractional abundance f of SB1 binaries would be

$$\frac{\sigma}{\sigma_0} = \sqrt{1 + f \left(\frac{\sigma_{\text{SB1}}}{\sigma_0} \right)^2} \sim \sqrt{f}.$$

However, in our case, the exponent in the dependence of the relative mean-square velocity on the fractional abundance f of SB1 binaries is less than 0.5 due to the non-Gaussian nature of the velocity distribution of the primary components of SB1 binaries (see Figure 5).

5. The Mass of NGC 2571

We used the velocity dispersion in the tangential direction to estimate the dynamical mass of NGC 2571. We assume that the velocity distribution in the line-of-sight direction is the same as the velocity distribution in both tangential directions and evaluate the squared velocity dispersion as $\sigma^2 = (3/2)(\sigma_\alpha^2 + \sigma_\delta^2)$.

To estimate the cluster mass, we follow Seleznev et al. (2017, Section 9.2). We estimate the virial cluster mass by the

formula

$$M_{\text{vir}} = \frac{2\sigma^2 \bar{R}}{G}, \quad (18)$$

and the cluster mass taking into account the gravitational field of the Galaxy and the cluster nonstationarity by the formula of Danilov & Loktin (2015):

$$M_d = \frac{2\bar{R}R_u \left[2\sigma^2 - \frac{(\alpha_1 + \alpha_3)\langle r^2 \rangle}{3} \right]}{G(\bar{R} + R_u)}, \quad (19)$$

where $R_u = \langle 1/r_i \rangle^{-1}$ is the mean inverse star distance to the cluster center, $\bar{R} = \langle 1/r_{ij} \rangle^{-1}$ is the mean inverse star-to-star distance, $\langle r^2 \rangle$ is the mean square of the star distance to the cluster center, α_1 and α_3 are the field constants (Chandrasekhar 1942) characterizing the Galactic potential, $\Phi(R, z)$, in Galactocentric cylindrical coordinates in the vicinity of a star cluster:

$$\alpha_1 = \left(\frac{1}{R} \frac{\partial \Phi}{\partial R} - \frac{\partial^2 \Phi}{\partial^2 R} \right)_{R_{cl}} = 4A(B - A) < 0, \quad (20)$$

where A and B are the Oort's constants, and

$$\alpha_3 = - \left(\frac{\partial^2 \Phi}{\partial^2 z} \right)_{z_{cl}} > 0. \quad (21)$$

R_{cl} and z_{cl} are the cluster center-of-mass cylindrical coordinates. The values of α_1 and α_3 were calculated adopting the Galactic potential model of Kutuzov & Osipkov (1980). Arguments in favor of this model are listed in Seleznev (2016a).

We performed the following steps to evaluate the cluster mass by Equations (18) and (19).

1. First, we determined the cluster radius following the method proposed in Seleznev (2016a). This method is based on the comparison of the surface density radial profile of the cluster with the mean density of surrounding field stars. The cluster radius is the distance from the cluster center where the radial density profile intersects the (horizontal) line of the mean density of field stars (see Seleznev 2016a for more details). Toward this aim, we have selected stars from the Gaia DR3 catalog (Gaia Collaboration et al. 2023) in a field $5^\circ \times 5^\circ$ around the cluster center in the parallax and proper-motion range of $\varpi \in [0.5; 1.0]$ mas, $\mu\alpha \in [-5.4; -4.5]$ mas yr $^{-1}$ and $\mu\delta \in [3.8; 4.7]$ mas yr $^{-1}$ with $G \leq 18$ mag, respectively, to minimize the field stars' contamination. The resulting cluster radius is $R_c = 87' 9 \pm 1' 3$. Then, the cluster is found to have a large corona with low stellar density. All this is illustrated in Figure 7, where the cluster radial density profile (solid black line) shows the cluster corona extending from approximately $20'$ to nearly $90'$. The outer radius of the cluster corona (the cluster radius) is determined as the first intersection of the radial density profile with the line of the mean density of the field stars (horizontal red line). This fact is confirmed by the map of the whole of Hunt & Reffert (2023) sample. This sample has an extended asymmetric corona of stars with a membership probability less than 0.5.

2. We fitted the surface density $F(r)$ in the cluster corona region by a second-order polynomial and obtained a steadily decreasing function.

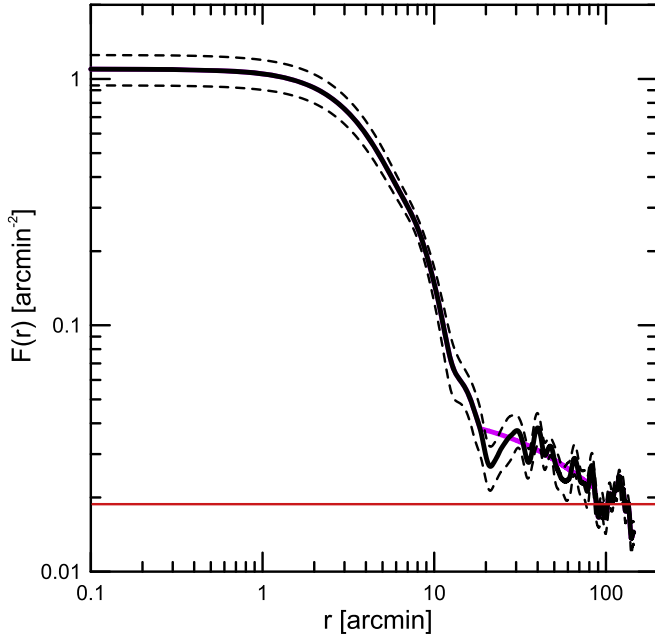


Figure 7. The surface density profile of NGC 2571, denoted by the solid black line. Dashed black lines show the confidence interval. The horizontal red line shows the mean field density. The smooth magenta line at the bottom right is a polynomial approximation of the surface density in the cluster corona.

3. We obtained the spatial distribution of stars $f(r)$ around the cluster center using the solution of the Abel equation proposed by von Zeipel & Lindgren (1921):

$$f(r) = \frac{1}{\pi} \int_0^{\sqrt{R_c^2 - r^2}} S(\sqrt{r^2 + z^2}) dz, \quad (22)$$

where

$$S(r) = -\frac{1}{r} \frac{dF(r)}{dr}. \quad (23)$$

4. To estimate the values of \bar{R} , R_u , and $\langle r^2 \rangle$, we performed a Monte Carlo sampling of the spatial density profile $f(r)$. Twenty different Monte Carlo samples were built in order to estimate the scatter in the estimates. We obtained $\bar{R} = 1.90 \pm 0.08$ pc, $R_u = 0.60 \pm 0.21$ pc, and $\langle r^2 \rangle = 5.39 \pm 0.31$ pc² for a cluster distance of 1293 pc (Dias et al. 2021).

5. Finally, we obtained $M_{\text{vir}} = 650 \pm 30 M_\odot$ and $M_d = 310 \pm 80 M_\odot$ using the velocity dispersion for the Cantat-Gaudin et al. (2020) sample of member stars. Masses corresponding to the Hunt & Reffert (2023) sample differ negligibly.

It is interesting to compare these estimates with the cluster photometric mass. We took the sample of the NGC 2571 probable members from Cantat-Gaudin et al. (2020) and the PARSEC isochrone (Bressan et al. 2012) of the age and metallicity corresponding to the cluster data from Dias et al. (2021). The stellar absolute magnitudes were obtained adopting distance and reddening from Dias et al. (2021). The lower estimate of the cluster photometric mass turned out to be $M_{\text{ph}} = 290 \pm 20 M_\odot$ for probable cluster members with magnitude $G \leq 18$ mag (this magnitude corresponds to approximately $0.7 M_\odot$). The uncertainty corresponds to the cluster distance and reddening errors from Dias et al. (2021). Also, we took into account the uncertainty of the mass obtained from the theoretical isochrone (Bressan et al. 2012) to be $0.11 M_\odot$.

The cluster photometric mass is in a rough agreement with the estimates of the cluster dynamical mass considering that we are neglecting weak invisible stars, dark remnants, and unresolved binary and multiple stars (see the analysis in Seleznev 2016a, Seleznev et al. 2017, and Borodina et al. 2021). We can evaluate the total cluster mass considering all these populations. The Cantat-Gaudin et al. (2020) sample has magnitudes in the range $G \in [8.7; 18]$. This magnitude range corresponds to the mass range of $m \in [0.71; 7.18] M_\odot$ considering the cluster distance and reddening from Dias et al. (2021) and the theoretical isochrone of Bressan et al. (2012) for the cluster age $\log t = 7.52$ (Dias et al. 2021). We assume that the total range of the stellar mass in the cluster at the beginning was $m \in [0.08; 60] M_\odot$ and use the Kroupa (2001) initial mass function.

We consider that stars with an initial mass less than $8 M_\odot$ evolve to white dwarfs (Limongi et al. 2024) with a mean mass of $0.79 \pm 0.16 M_\odot$ (Suleimanov et al. 2019). Stars with an initial mass $m \in [8; 27] M_\odot$ and solar metallicity explode as supernovae (Heger et al. 2003) and leave neutron stars with a mean mass of $1.4 M_\odot$. Stars with an initial mass $m \in [27; 65] M_\odot$ and solar metallicity also explode as supernovae (Heger et al. 2003) but leave black holes with a relatively small mass (Heger et al. 2003). The latter evolutionary path is the most ambiguous since the exact mass loss is unknown. For the sake of simplicity, we assume that the mass of the black hole is equal to one-half of the progenitor's mass.

Finally, we take into account the presence of unresolved binary and multiple stars following the scheme described in Borodina et al. (2021). As for the fractional abundance of the unresolved binary and multiple stars, we assume it to be similar as in the Alpha Persei cluster, $\alpha = 0.48$ (Malofeeva et al. 2022), which is the closest in age among the four clusters studied in Malofeeva et al. (2022). According to Borodina et al. (2021), the cluster mass increment is approximately 1.2. This yields a total cluster mass estimate of $700 \pm 200 M_\odot$.

We have estimated the spread of the total cluster mass estimate by a numerical experiment. To do this, we performed an estimate of the total cluster mass (see above) 1000 times varying the exponents of the Kroupa (2001) mass function and the *visible* cluster mass ($M_{\text{ph}} = 290 \pm 20 M_\odot$). All varying values were considered as distributed by a Gaussian law; their errors were used as a standard deviation.

The resulting distribution is skewed (with a long tail toward large values of mass) with a mode of approximately $700 M_\odot$. As an associated error, we assume the standard deviation obtained after the removal of values exceeding the mode by 3 times the initial standard deviation.

The estimate of $700 \pm 200 M_\odot$ has been derived adopting the Kroupa (2001) initial mass function, but the cluster's actual total mass is expected to be somewhat smaller due to dissipation during the relaxation phase.

In conclusion, this photometric estimate of the total cluster mass is in good agreement with the estimate of the cluster dynamical mass.

6. Summary and Conclusions

In this study, we present a method to estimate the mean-square velocity of star cluster probable members from radial velocities and proper-motion measurements, taking into account the errors of these values. To do this, we assume that

the errors follow a normal distribution and use the properties of the convolution of several normal distributions.

In particular, we consider the mean-square velocity of the probable members of the open cluster NGC 2571 obtained from radial velocities obtained at the VLT telescope and from Gaia DR3 proper motions. The mean-square velocity considering radial velocities only (line-of-sight mean-square velocity) turns out to be 6–8 times larger than the mean-square velocity derived from proper-motion components only (the tangential mean-square velocity). We have shown that the larger value of the line-of-sight mean-square velocity can be explained by the pollution of the sample with the radial velocities of spectroscopic binaries with spectral lines of the primary component (SB1) only. These binaries cannot be distinguished from single stars with just single-epoch observations. Figure 6 shows that a fractional abundance, f , of SB1 binaries of just 0.2 leads to an overestimation of the mean-square velocity of a factor around 2.3. In turn, the squared mean-square velocity (and hence the cluster virial mass) will be overestimated by about 5.3 times.

In the specific case of NGC 2571, we have estimated both the virial mass and the mass resulting from the formula of Danilov & Loktin (2015) using the mean-square velocity from the proper motions only. Both values are in substantial agreement with the photometric mass, derived accounting for the star cluster probable members.


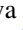
Li et al. (2020) showed that proper motions also can be influenced by unresolved binaries. However, this influence seems to be negligible given the substantial agreement between NGC 2571's photometric and member-based dynamical mass.

Our results demonstrate that one can use radial velocities to estimate the mass of a star cluster only after carefully cleaning for spectroscopic binaries.

Acknowledgments

This work is based on observations carried out at ESO Paranal Observatory under program 096.B-0004(A). This work has made use of data from the European Space Agency (ESA) mission Gaia (<https://www.cosmos.esa.int/gaia>), processed by the Gaia Data Processing and Analysis Consortium (DPAC, <https://www.cosmos.esa.int/web/gaia/dpac/consortium>). Funding for the DPAC has been provided by national institutions, in particular the institutions participating in the Gaia Multilateral Agreement. The work of M.V.K. and A.F.S. was supported by the Ministry of Science and Higher Education of the Russian Federation by an agreement FEUZ-2023-0019.

ORCID iDs

Maxim V. Kulesh  <https://orcid.org/0000-0003-2125-8740>
 Giovanni Carraro  <https://orcid.org/0000-0002-0155-9434>
 Joao V. Sales-Silva  <https://orcid.org/0000-0003-0636-7463>
 Anton F. Seleznev  <https://orcid.org/0000-0001-8669-803X>

References

- Blecha, A., Cayatte, V., North, P., Royer, F., & Simond, G. 2000, *Proc. SPIE*, **4008**, 467
- Borodina, O. I., Carraro, G., Seleznev, A. F., & Danilov, V. M. 2021, *ApJ*, **908**, 60
- Borodina, O. I., Seleznev, A. F., Carraro, G., & Danilov, V. M. 2019, *ApJ*, **874**, 127
- Bressan, A., Marigo, P., Girardi, L., et al. 2012, *MNRAS*, **427**, 127
- Cantat-Gaudin, T., Anders, F., Castro-Ginard, A., et al. 2020, *A&A*, **640**, A1
- Chandrasekhar, S. 1942, *Principles of Stellar Dynamics* (Chicago, IL: Univ. Chicago Press)
- Danilov, V. M., & Loktin, A. V. 2015, *AstBu*, **70**, 414
- Dias, W. S., Monteiro, H., Moitinho, A., et al. 2021, *MNRAS*, **504**, 356
- Eker, Z., Soydogan, F., Soydogan, E., et al. 2015, *AJ*, **149**, 131
- Gaia Collaboration, Brown, A. G. A., Vallenari, A., et al. 2018, *A&A*, **616**, A1
- Gaia Collaboration, Prusti, T., de Bruijne, J. H. J., et al. 2016, *A&A*, **595**, A1
- Gaia Collaboration, Vallenari, A., Brown, A. G. A., et al. 2023, *A&A*, **674**, A1
- Gray, D. F. 1976, *The Observation and Analysis of Stellar Photospheres* (New York: Wiley)
- Heger, A., Fryer, C. L., Woosley, S. E., Langer, N., & Hartmann, D. H. 2003, *ApJ*, **591**, 288
- Hunt, E. L., & Reffert, S. 2023, *A&A*, **673**, A114
- Jeans, J. H. 1919, *MNRAS*, **79**, 408
- Kroupa, P. 2001, *MNRAS*, **322**, 231
- Kutuzov, S. A., & Osipkov, L. P. 1980, *SvA*, **24**, 17
- Li, L., Shao, Z., Li, Z.-Z., et al. 2020, *ApJ*, **901**, 49
- Limongi, M., Roberti, L., Chieffi, A., & Nomoto, K. 2024, *ApJS*, **270**, 29
- Malofeeva, A. A., Seleznev, A. F., & Carraro, G. 2022, *AJ*, **163**, 113
- Merritt, D., & Tremblay, B. 1994, *AJ*, **108**, 514
- Munari, U., Sordo, R., Castelli, F., & Zwitter, T. 2005, *A&A*, **442**, 1127
- Rastello, S., Carraro, G., & Capuzzo-Dolcetta, R. 2020, *ApJ*, **896**, 152
- Seleznev, A. F. 2016a, *MNRAS*, **456**, 3757
- Seleznev, A. F. 2016b, *BaltA*, **25**, 267
- Seleznev, A. F., Carraro, G., Capuzzo-Dolcetta, R., Monaco, L., & Baume, G. 2017, *MNRAS*, **467**, 2517
- Silverman, B. W. 1986, *Density Estimation for Statistics and Data Analysis* (London: Chapman and Hall)
- Suleimanov, V. F., Doroshenko, V., & Werner, K. 2019, *MNRAS*, **482**, 3622
- Taboga, M. 2017, *Lectures on Probability Theory and Mathematical Statistics* (3rd ed.; North Charleston, SC: CreateSpace)
- Tonry, J., & Davis, M. 1979, *AJ*, **84**, 1511
- Tutukov, A. V., & Kovaleva, D. A. 2019, *INASR*, **3**, 342
- von Zeipel, H., & Lindgren, J. 1921, *KSVH*, **61**, 15